Web Crippling Behaviour and Design of Aluminium Lipped Channel Sections under Two Flange Loading Conditions

Husam Alsanat
School of Engineering and Built Environment, Griffith University
Gold Coast, QLD, 4222, Australia.
School of Engineering, Al-Hussein Bin Talal University, Ma'an, Jordan.

Shanmuganathan Gunalan
School of Engineering and Built Environment, Griffith University
Gold Coast, QLD, 4222, Australia.

Pologanathan Keerthan
Faculty of Engineering and Environment, University of Northumbria,
Newcastle, UK.

Hong Guan
School of Engineering and Built Environment, Griffith University
Gold Coast, QLD, 4222, Australia.

Konstantinos D. Tsavdaridis
School of Civil Engineering, University of Leeds, LS2 9JT, Leeds, UK

Abstract

Aluminium alloys have recently drawn significant attention in structural applications due to its outstanding mechanical characteristics. Thin-walled members fabricated by aluminium alloys can be more competitive in construction industries than the conventional cold-formed steel sections, particularly in areas with high humidity and severe environmental conditions. Nevertheless, they are more vulnerable to various types of instability due to their relatively low elastic modulus compared to steel. Applying high concentrated load transversely on thin-walled members can cause critical damage to the web of the cross section called web crippling. Although a large number of studies has been performed to investigate the web crippling mechanisms on different types of sections, the existing studies are primarily of the empirical nature and thus merits further investigations. To fill the research gap, this study was thus performed based on our previously conducted experimental work to further comprehend the web crippling phenomenon of the roll-formed aluminium lipped channel (ALC) sections under the loading conditions of end-two-flange (ETF) and interior-two-flange (ITF). This was done through numerical investigations followed by a parametric study which are reported herein in details. A wide range of roll-formed ALC sections covering web slenderness ratios ranged from

28 to 130, inside bent radii ranging between 2 mm and 8 mm, bearing lengths ranged from 50 mm to150 mm, and three sheeting aluminium alloy grades (5052-H32, 5052-H36 and 5052-H38) were considered in the parametric study. The acquired web crippling database was then used to assess the consistency and accuracy of the current design rules used in practice. It was found that the web crippling capacity determined by the current international specifications are unsafe and unreliable, whereas the predictions of the recently proposed equations agree very well. Furthermore, a Direct Strength Method (DSM)-based capacity prediction approach was proposed and then validated against the web crippling database acquired here as well as the experimental and numerical data for cold-formed steel lipped channel sections used in the literature.

Keywords: Roll-formed; Aluminium; Lipped Channel Sections; Web Crippling; Design Rules; Direct Strength Method.

Nomenclature

b_f	flange width
C	web crippling coefficient
C_b	general coefficient for buckling
$C_{b,b}$	coefficient of flange width to thickness ratio for buckling
$C_{b,N}$	coefficient of bearing length to thickness ratio for buckling
$C_{b,r}$	coefficient of inside bent radius to thickness ratio for buckling
$C_{b,w}$	coefficient of web slenderness ratio for buckling
C_h	web slenderness coefficient
C_n	correction factor depending on the number of tests
C_N	bearing length coefficient
C_R	inside corner radius coefficient
d	web (total) height
d_w	web height between flange mid-lines
E	Young's modulus of elasticity
E_{sh}	strain hardening slope
F_m	mean value of fabrication factor
f_u	ultimate stress
f_y	yield stress
h	web (flat) height
k_{cr}	buckling coefficient
L	specimen length
l_b	lip length
M_m	mean value of material factor
n	number of tests
N	load bearing length
N_m	plastic mechanism length
P_{AS1664}	ultimate load obtained from Eqs. (5 and 6)
P_{AS4600}	ultimate load obtained from Eq. (7)

P_{cr}	buckling load
P_{EC3}	ultimate load obtained from Eqs. (8 and 9)
$P_{Exp.}$	ultimate load obtained from experimental test
P_{FEA}	ultimate load obtained from FEA
P_m	mean value of tested-to-predicted load ratio
P_n	ultimate load obtained from DSM approach
$P_{Predicted}$	ultimate load obtained from equation
$P_{unified}$	ultimate load obtained from Eq. (10)
P_y	plastic load
r_{ext}	external bent radius
r_i	inside bent radius
r_m	inside bent radius
t	thickness
V_F	coefficient of variation of fabrication factor
V_m	coefficient of variation of material factor
V_p	coefficient of variation of tested-to-predicted load ratio
V_Q	coefficient of variation of load effect
$\propto$	coefficient for various local loads and support categories
λ	the web crippling slenderness ($\lambda = \sqrt{P_y/P_{cr}}$)
β_0	reliability index
ε_{eng}	engineering strain
ε_{true}	true strain
ε_u	ultimate strain
ε_y	yield strain
σ_{eng}	engineering stress
σ_{true}	true stress
θ	angle between the plane of web and the plane of bearing surface
ϕ_w	resistance (capacity) factor
γ_{M1}	partial safety factor

1 Introduction

Over the last two decades, aluminium alloys have been productively used in construction industries as a thin-walled structural member due to its advanced mechanical properties. Several attempts have been made to utilise aluminium in construction [1-2], and it has been well recognised that aluminium alloys have economic advantages, and are therefore competitive, in structural applications where their inherent characteristics including low density (third of steel density), corrosion resistance and functionality of structural shape are fully utilised. Moreover, the physical properties, technological features and production process of aluminium alloys have improved their prospect to compete with steel in a wide range of building applications especially those in harsh industrial and marine environments [3, 4].

In general, thin-walled flexural members are highly prone to various types of buckling instabilities including local, distortional and global buckling. Inducing high concentrated loads

or reactions transversely on the members may potentially lead to a critical failure on the web of the cross section called web crippling. Besides the extensive experimental investigations conducted to explore the web crippling phenomenon, numerical analyses have also been implemented to further comprehend the mechanism of web crippling failure on various section types. It has been recognised that such analyses are more flexible in offering much detailed quantitative results, hence saving a great deal of time and effort compared with the experimental work. In the literature, several attempts have been conducted to investigate the web crippling failure numerically using different analysis methods. Macdonald et al. [5] and Ren, et al. [6] carried out a nonlinear finite element (FE) analysis using ANSYS software on cold-formed channels under web crippling action. Non-Linear static analysis was performed showing detailed model definitions, particularly those related to the boundary conditions and symmetry. Yousefi et al. [7] also employed a similar analysis approach, implicit quasi-static analyses, using ABAQUS to simulate the web crippling behaviour of cold-formed ferritic stainless steel unlipped channels with web holes. Recently, an explicit quasi-static analysis method in ABAQUS was successfully employed to investigate the web crippling strengths of cold-formed steel members [8-10]. It was found that this type of analysis is more effective in overcoming specific convergence issues often encountered in the nonlinear static analysis method.

Even though aluminium alloys share many similarities with steel, the application of the design methods developed for steel, being empirical in nature, may not be possible for aluminium elements [11]. Therefore, several studies have been undertaken to investigate the web crippling actions on aluminium members. Zhou and Young [12, 13] carried out experimental web crippling tests using extruded aluminium hollow sections with/without a circular hole in the webs. The tests were conducted under two flange loading conditions (ETF and ITF) where the bearing plates were unfastened to the section flanges. Numerical models were developed and non-linear static analyses were performed. The numerical results were then validated against the experiments. Similarly, experimental and numerical investigations were reported by Chen, et al. [14] to assess the web crippling failure of extruded aluminium hollow sections under one and two flange loading conditions. Wang et al. [15] performed both experimental study and numerical analysis of web crippling of extruded I-shaped aluminium alloy beams under one flange load cases. Non-linear finite element analysis using the Arc-Length Method in ANSYS was employed. Recently, Su and Young [16] investigated the web crippling failure for extruded aluminium stocky hollow sections under the four loading conditions. Numerical models were

developed and verified against the experiments and subsequently used to conduct a parametric study.

Since most of the available studies on aluminium members are limited to extruded symmetrical sections (hollow and I-shaped sections), further research and design guidelines are required to estimate the web crippling strengths of roll-formed asymmetrical aluminium alloy sections based on a large number of experimental and numerical results.

In this study, accurate nonlinear finite element (FE) models were developed first for roll-formed ALC sections subject web crippling under the ETF and ITF loading conditions. The developed FE models were then verified against the experimental data reported in Alsanat et al. [17]. The outcomes of this study indicate that the numerical results agreed well with the experiments in terms of the ultimate web crippling strengths, load-vertical displacement responses, and failure modes. Based on the verified FE models, a comprehensive parametric study covering wide-ranged ALC dimensions, aluminium alloy grades, and bearing lengths was conducted. The acquired parametric database including all relevant experimental and FE results was then used to evaluate the consistency and reliability of the currently used design rules [17-20]. Furthermore, a Direct Strength Method (DSM) design approach was proposed based on a consistent elastic buckling and plastic analysis to determine the web crippling capacities of both roll-formed aluminium and cold-formed steel lipped channel members under the two flange loading conditions.

2 Brief overview of experimental study

Alsanat et al. [17] undertook a web crippling experimental study comprising forty tests (including two repeated tests) on ALC sections under two flange loading conditions (ETF and ITF). The specimens were roll-formed using the structural aluminium alloy grade 5052 H36. The test set-up and the specimen length were designed according to the AISI Standard test method [21] for cold-formed steel structures, as shown in Figure 1. The experiments covered five different lipped channel sections with four bearing plate lengths (N ranged from 25 mm to 150 mm) for both the ETF and ITF loading conditions. The average measured geometric dimensions of the tested sections are given in Tables 1 and 2, with the member length equal three and five times the section depth (d) for the ETF and ITF loading conditions, respectively. During the test, the flanges of the lipped channel specimens were not attached to the supports (bearing plates).

The specimens were labelled in a way that the loading condition, web height and thickness, and the bearing plate length could be easily known from the label. For example, the label "ITF-10030-N50" indicates that the specimen's load case is ITF, the web height is 100 mm, the web thickness is 3 mm, and the bearing length (N) is 50 mm.

3 Numerical study

In order to simulate the ALC sections subjected to web crippling, the finite element and general purpose analysis program ABAQUS version 6.14 [22] was employed in this study. As mentioned earlier, two analysis methods were employed in the previous FE studies of web crippling, namely: non-linear static analysis and explicit quasi-static analysis methods. The latter was chosen in this study to investigate the web crippling mechanism of the ALC section due to its ability to overcome the difficulties associated with convergence and contact that non-linear static analyses often encounter [8,10].

3.1 FE model development

The FE models in this study consist of three main components namely: the ALC section, the bearing plates and the contact between them. The cross-sectional dimensions and properties of material acquired from the coupon tests reported in [17] were implemented to develop the numerical models. The influence of initial geometrical imperfections on the ultimate web crippling capacities of cold-formed steel lipped channel sections under two-flange load cases was thoroughly investigated by Natário, et al. [8] and Sundararajah et al. [10]. Several initial geometrical imperfection situations were explored, and it was concluded that their overall effect on the web crippling capacity is barely perceptible (less than 1%). Given the fact that the web moment caused by the geometrical eccentricity (due to corner radius) is relatively larger than that induced by the presence of initial geometrical imperfections, and such imperfections of the ALC specimens were thus not considered in this study.

3.1.1 Finite element type and mesh control

There are several options of element types that are available in the ABAQUS element library [22]. In this study, four shell element types including S4, S4RS, S4R, and S4RSW were investigated. Specimen ETF-10030-N50 was chosen as a benchmark to study the influence of the element type on the behaviour and capacity of web crippling. Figure 2 shows the comparison of the load-displacement curves for these types of shell elements. It is shown that the ultimate web crippling capacities predicted using S4, S4R and S4RS elements closely

match with test results; however, the simulated capacity using S4RSW element is significantly lower than the test result. In this study, therefore, the ALC sections were modelled using the S4R shell elements as recommended by [8-10], while the rigid bearing plates were modelled using R3D4 element which is a bilinear 4-node 3-D rigid quadrilateral element.

Suitable sizes of the finite element mesh for web, flanges and the corners were selected depending on the result accuracy and the computational time of the analyses. To determine the most appropriate mesh size, ETF-10030-N50 was modelled using element mesh sizes ranged from 3 mm×3 mm to 20 mm×20 mm. Figure 3 shows the load versus vertical displacement curves for ETF-10030-N50 specimen with various mesh sizes. It is shown that the capacity of web crippling is not significantly affected by the mesh size. However, it is clearly seen from Figure 4 that 5 mm×5 mm mesh size is the most suitable size with satisfying computational time. Hence, the mesh size of 5 mm×5 mm was used for the flanges and the web while finer mesh (5 mm×1 mm) was used for the corners of the section to ensure proper transformation of the load from the flange to the web of the section.

3.1.2 Material properties

The specimens' material properties measured from the coupon tests [17] were used in the FE analyses. Since high plastic strains are expected to occur in web crippling problems, it is recommended to use the true stress-logarithmic strain curve by converting the usual (engineering) stress-strain curve using the following equations:

$$\sigma_{true} = \sigma_{eng}(1 + \varepsilon_{eng}) \quad (1)$$

$$\varepsilon_{true} = ln(1 + \varepsilon_{eng}) \quad (2)$$

where σ_{true} is the true stress (MPa), ε_{true} is the true strain, σ_{eng} is the engineering stress (MPa) and ε_{eng} is the engineering strain.

The converted true stress and strain values were used herein to define the material properties in the numerical models. Figure 5 shows the typical true stress-strain curve for the 5052 H36 aluminium alloy. It should be noted that the plastic deformation of corners due to the roll-forming process was not considered in the material model in this study. This is due to the fact that the scope of this study is focused on the failure of the web (web crippling) in the lipped channel sections. Hence the material properties used throughout the sections were based on the tensile coupon tests conducted using the samples from the web element. Similar approach was used in the previous numerical studies [8,10] on cold-formed steel lipped channel sections.

3.1.3 Contact definition

There are two common algorithms to model contact in ABAQUS, so-called General Contact and Contact Pair algorithms. The latter was used in this study to simulate a pure master-to-slave contact with Kinematic Contact method due to its suitability to simulate the contact between rigid elements (bearing plates) and deformable bodies (aluminium sections). The contact formulation was assumed to be "Hard" in the developed numerical models as the bearing plates were nondeformable.

To avoid any fractional slip during the analyses, friction between the contact bodies was defined. The influence of various friction coefficients was explored, and it was found that their effect on the web crippling capacity and behaviour of the ALC sections was minimal. Hence, a friction coefficient of 0.4 was assumed for all the numerical models.

3.1.4 Boundary conditions

The boundary conditions were assigned to the loading plates using Reference Points (RP) as shown in Figure 6. The ETF boundary conditions were similar to those applied to the ITF models. As illustrated in the figure, all the translational displacements (U_x, U_y and U_z) and rotations (R_y and R_z) except for the rotational degree about the X-axis (R_x) were fixed at the support plate (bottom plate). The loading plate (top plate) was prevented from translational displacement in U_x and U_z directions and rotations R_y and R_z. However, the translational displacement U_y was allowed to move vertically with a limited 25 mm displacement towards the specimen.

A Smooth Step Amplitude option was implemented in the boundary condition of the loading plate to impose a transverse load on the sample. This option allows the specimen to deform in a smooth manner from the original state as the displacement in the initial phase was slower. It should be mentioned that the required stable time increment for the quasi-static analyses is several orders of magnitude smaller than the experimental time which leads to the generation of a very large number of calculations. To reduce the computational time, the mass density of the elements was increased using 'Mass Scaling' method to raise the stability limit and to significantly reduce the number of increments.

3.2 FE analysis validation

A total of 38 ALC sections under the web crippling action were numerically analysed and compared with the experimental results. Tables 1 and 2 show a strong agreement between the

experimental web crippling capacities ($P_{Exp.}$) and the FE results (P_{FEA}) for both ETF and ITF loading conditions, respectively. The mean value of the $P_{Exp.}/P_{FEA}$ ratio for both the ETF and ITF specimens is 1.00 with the COV value of 0.05 for the ETF loading condition and 0.03 for the ITF loading condition.

The load-vertical displacement curves derived from the numerical analyses and the failure modes were also compared with the experimental measurements and observations (Figures 7 (a) and (b)). Although the ultimate and post-failure stages agree very well, a noticeable difference in the elastic stiffness was found in the pre-failure stage. It is believed that such a difference was due to the flexibility of the test rig, which was inevitably included when measuring the vertical displacement during the tests. Figures 8 (a) and (b) compare the failure modes of the ETF-20025-N50 and ITF-25025-N50 specimens, respectively. Generally, the comparisons indicate that the numerical models are able to reproduce the experimental ultimate web crippling capacities, load-vertical displacement responses and failure modes of the ALC sections under two flange loading conditions.

It was also observed from the experimental investigations [17] that all the ITF specimens with a small loading plate (N= 25 mm) underwent a combined web crippling and flange crushing failure. The developed numerical models were also validated against the experiments of such kind of failure. Numerical load-vertical displacement plots and failure modes were compared in Figures 7 and 8, respectively, with the experimental results of specimens exhibited flange crushing failure. Figure 7 (c) shows the applied load-vertical displacement curves obtained from the test and the FE analysis for the ITF-10030-N25 section. The two curves agree well from the initiation of the test until the occurrence of flange crushing. Figure 8 (c) presents the failure modes of ITF-15025-N25 as observed from the experiments and the FE analysis.

4 Parametric study

In this research, a detailed paramedic study was performed to thoroughly investigate the web crippling phenomenon of the ALC sections under two-flange loading conditions. The validated FE models were used as a basis for the paramedic study to create a comprehensive web crippling capacity database. This database will then be used to investigate the accuracy of the available design guidelines obtained from the international specifications and Alsanat et al.'s [17] modified equations. Furthermore, DSM-based capacity prediction equations will be proposed and calibrated based on this database.

4.1 Minimum control specimen length

It was observed from the experimental results that all the specimens subjected to the ITF loading condition and with 100 and 150 mm bearing plates were unable to reach their ultimate potential web crippling strengths [17], given the fact that the influence zone length was extended to more than that the specimens length recommended by the AISI Standard [21]. To investigate this issue numerically, von Mises stress distributions and the load versus displacement curves for the 25025-N100 and 25025-N150 specimens, respectively, with different bearing plate lengths were compared. Figures 9 (a-d) display the von Mises stress distributions at the maximum loads of the 25025-N100 specimen with two sets of lengths: *3d* and *4d* for the ETF loading condition, as well as *5d* and *6d* for the ITF loading condition. For the ETF loading condition, it is clearly observed that the stresses at the free specimen end remain at the negligible values for both lengths. Therefore, it can be confirmed that the recommended control length of the ETF specimens ($L \geq 3d$) for cold-formed steel sections is suitable for aluminium members as well.

For the ITF loading condition, however, the stresses with a *5d* length reached rather high values at both ends, while they are relatively low for the specimen with a *6d* length. Figure 10 presents the typical load versus vertical displacement curves for specimen ITF-25025-N150 with different lengths. A significant drop in the web crippling capacity can be clearly seen in the specimen with the control length ($L=5d$) in comparison with the longer specimens. Hence, a parametric study was conducted to determine an appropriate minimum length for the ALC sections under the ITF loading condition. A total of thirty-six FE models loaded by 100 mm and 150 mm bearing plate lengths were established with different specimen lengths ($L = 5d$, *6d*, *9d* and *13d*) under the ITF loading condition. The ultimate web crippling strengths of these models are given in Table 3. The ultimate strength ratios of the numerical models with the control length ($L=5d$) with respect to those of $L=13d$ were found to reach as low as 88%. However, the capacity ratios for the specimens of a *6d* length are more conservative with a minimum value of 97% and this ratio is 98% for the specimens with control length ($L=9d$). Thus, it is recommended to increase the minimum specimen length to six times the section height for any future web crippling studies using aluminium sections.

4.2 Web crippling parameters

Table 4 summarises the details of the parametric study conducted for the ALC sections under the ETF and ITF loading conditions. Bearing lengths (N) ranging from 50 mm to150 mm, inside

bent radius (r_i) ranging from 2 mm to 8 mm and web slenderness (h/t) ranging from 27.7 to 130 were considered to investigate their effects on the web crippling failure. Furthermore, up to three different aluminium alloy grades: 5052-H32 (yields stress (f_y) = 145 MPa, ultimate stress (f_u)= 214 MPa and Young's Modulus (E) = 70 GPa), 5052-H36 (f_y = 179MPa, f_u = 255 MPa and E = 69.3 GPa) and 5052-H38 (f_y = 207 MPa, f_u = 268 MPa and E = 70.3 MPa) [18] were also considered in this study to investigate the effects of the material properties of different aluminium alloy grades. Note that the specimen's length was *3d* for the ETF loading conditions and *6d* (the proposed length) for the ITF loading condition. Also, this parametric study does not include the small bearing length (N = 25 mm) as the numerical models may gain more capacity due to flange crushing (yielding of the web-flange corner region).

The bi-linear material model implemented by Su et al. [23] for the development of the Continuous Strength Method (CSM) to design aluminium alloy structures was used here to represent the material properties in the parametric FE analyses. Typically, this model considers the strain hardening of the aluminium material and consists of two stages: the initial elastic stage, represented by the Elastic modulus of the material E, and the linear hardening stage with a strain hardening slope (E_{sh}), determined by Equation (3). The ultimate strain (ε_u) can be calculated using Equation (4).

$$E_{sh} = \frac{f_u - f_y}{C_2 \varepsilon_u - \varepsilon_y} \tag{3}$$

$$\varepsilon_u = C_3 \left(1 - \frac{f_y}{f_u}\right) + C_4 \tag{4}$$

where ε_y is the yield strain, f_u is the material ultimate strength (MPa), and C_2 = 0.5, C_3 = 0.13, and C_4 = 0.059 are set for aluminium alloys. Figure 5 compares the typical material stress-strain curve and the CSM material bilinear model.

Figures 11 to 14 illustrate the influences of the main web crippling parameters on the overall capacities of the ALC sections under the ETF and ITF loading conditions. Figure 11 shows an inverse relationship between the web slenderness ratio (h/t) and the ultimate web crippling capacity of the ALC sections with three different bearing lengths (N). It can be seen that the sections with a small slenderness ratio (h/t = 32) are more sensitive to the bearing length variations compared to a large slenderness ratio (h/t = 125). Moreover, the sections loaded by smaller bearing plates have a smoother reduction in capacity compared to those with large bearing plates. Figure 12 demonstrates the effects of the loading plate length ratio (N/t) on the ultimate web crippling capacities of the ALC sections with varying internal corner radii (r_i) of 2, 5 and 8 mm. The section capacities are considerably increased when the N/t ratio increases

from 16 to 50, due to the increased distribution of the stresses generated from the bearing plates. It is also observed that such an increase is more sensitive with smaller r_i when the specimens are loaded under the ITF loading condition in comparison to the ETF loading condition. With respect to the varying internal bent radius ratios (r_i/t), it can be deduced from Figure 13 that an increase in r_i/t leads to a substantial reduction in the capacities of the ALC sections under both the ETF and ITF loading conditions. Given the fact that the out-of-plane bending moment acting on the flat portion of the web plate due to the eccentric load leads to a substantial reduction in the section capacity. Furthermore, the smaller the h/t ratio, the more significant the capacity reduction, especially under the ITF loading condition. Finally, it was observed from Figure 14 that increasing the yield strength (f_y) rises the capacities of the ALC sections in a linear manner, as expected, for all the specimens of three different bearing lengths (N) and under the loading conditions of both ETF and ITF loading conditions.

5 Current design rules

The web crippling strengths database created by the experimental and numerical parametric analysis results were compared with the predicted web crippling capacities calculated using the current design guidelines recommended in the AS/NZS 1664.1 [18], AS/NZS 4600 [19] and Eurocode 3 [20] specifications. It should be noted that the comparison excludes the design rules given in Eurocode 9 [24] Part 1.4 for cold-formed aluminium structures since they are limited to aluminium structural sheeting (members with two or more webs) and do not have the ability to estimate the web crippling capacity of single-web sections including aluminium lipped channel sections.

- **AS/NZS 1664.1 [18] for aluminium structures**

$$P_{AS1664} = \frac{1.2t^2 \sin\theta(0.46f_y+0.02\sqrt{Ef_y})(N+C_{w2})}{C_{w3}+r_i(1-\cos\theta)} \quad \text{(ETF)} \quad (5)$$

$$P_{AS1664} = \frac{t^2 \sin\theta(0.46f_y+0.02\sqrt{Ef_y})(N+C_{w1})}{C_{w3}+r_i(1-\cos\theta)} \quad \text{(ITF)} \quad (6)$$

where $C_{w1} = 140mm$; $C_{w2} = 33\,mm$; $C_{w3} = 10\,mm$; N is the bearing length (mm), f_y is the 0.2% static yield stress (MPa), E is the elastic modulus (MPa), t is the thickness of the web (mm), r_i is the internal corner radius (mm) and θ is the angle that is calculated from the bearing surface plane to the plane of the web surface. Note that θ is taken as 90^o for the lipped channel sections used in this experimental study.

- **AS/NZS 4600 [19] for cold-formed steel structures**

$$P_{AS4600} = Ct^2 f_y \sin\theta \left(1 - C_R\sqrt{\frac{r_i}{t}}\right)\left(1 + C_N\sqrt{\frac{N}{t}}\right)\left(1 - C_h\sqrt{\frac{h}{t}}\right) \quad (7)$$

where h is the flat portion of the web (mm); C is the general coefficient, C_R is the coefficient for the internal corner radius, C_N is the coefficient for the bearing length and C_h is the coefficient for the slenderness of the web. The values of these coefficients are shown in Table 5. Note that in Equation (7), the following conditions $h/t \leq 200$, $N/t \leq 210$, $r_i/t \leq 3$, $N/h \leq 2$, and $\theta = 90^o$ must be satisfied.

- **Eurocodes 3 [20] for cold-formed steel structures**

$$P_{EC3} = \frac{k_1 k_2 k_3 f_y t^2}{\gamma_{M1}}\left[6.66 - \frac{d_w}{64t}\right]\left[1 + 0.01\frac{N}{t}\right] \quad (8)$$

$$P_{EC3} = \frac{k_3 k_4 k_5 f_y t^2}{\gamma_{M1}}\left[21 - \frac{d_w}{16.3t}\right]\left[1 + 0.0013\frac{N}{t}\right] \quad (9)$$

where:

$k_1 = 1.33 - \frac{f_y}{690.9}$;

$k_2 = 1.15 - 0.15\frac{r_i}{t}$ $(0.5 \leq k_5 \leq 1.0)$;

$k_3 = 0.7 + 0.3\left(\frac{\theta}{90}\right)^2$;

$k_4 = 1.22 - \frac{f_y}{1036.4}$;

$k_5 = 1.06 - 0.06\frac{r_i}{t}$ $(k_5 \leq 1.0)$;

d_w is the web height between flange mid-lines in mm; γ_{M1} is the partial safety factor ($\gamma_{M1} = 1$) and θ is equal to 90^o.

Table 6 summarises the mean and COV values of capacity ratios $P_{Exp.\text{-}FEA}/P_{predicted}$, where $P_{Exp\text{-}FEA}$ is the ultimate capacities acquired from the experiments ($P_{Exp.}$) and numerical analyses (P_{FEA}) and $P_{predicted}$ is the predicted web crippling capacities yielded by the current international specifications. Generally, the design rules due to the aforementioned three specifications overestimate the web crippling strengths of the ALC sections, with the mean values ranging from 0.44 to 0.89, and large COV values from 0.13 to 0.47 for both the ETF and ITF loading conditions. The reasons behind such a gross overestimation of the web crippling capacity of channel sections based on the aforementioned specifications are: (i) both AS/NZS 4600 [19] and Eurocodes 3 [20] spesifications were developed for cold-formed steel sections and the

influence of the elastic modulus (E) was not considered, thus highly overestimating the capacity of aluminium sections, and (ii) the empirical design guideline given in the AS/NZS 1664.1[18] specification was developed based on the available experiments in the literature which were conducted using extruded and symmetrical sections (hollow and I shaped sections). Such sections can sustain more capacity compared to asymmetrical sections (channel sections) which experience high out-of-plane moment acting on the web due to eccentric loading. Figures 15 (a) and (b) display the comparison between the web crippling capacities $P_{Exp.-FEA}$ and $P_{predicted}$ of the current international specifications under the ETF and ITF loading conditions, respectively.

Alsanat et al. [17] considerably improved the accuracy of the design guidelines specified in the AS/NZS 1664.1 [18] and Eurocode 3 [20] specifications. This improvement was done by modifying the design equations according to their experimental results, where the slenderness ratio h/t of the test specimens ranged from 31 to 101, an inside bent radius limited to r_i = 5 mm and an aluminium alloy grade limited to 5052 H36. In the present study, a comparison between the predictions of the modified equations and those of the wide-ranged parametric analysis data obtained in Section 4 (including three aluminium alloy grades, h/t ranging from 28 to 130 and r_i = 2, 5 and 8 mm) and the experimental data were carried out. The comparison shows that the modified equations developed by Alsanat et al. [17] have the ability to precisely predict the web crippling strengths with reasonably acceptable mean and COV values of $P_{Exp.-FEA}/P_{predicted}$, ranging between 1.00 to 1.10 and 0.07 to 0.12, respectively, for both loading conditions as shown in Table 6.

The unified Equation (10) associated with the geometrical coefficients given in Table 5 was also proposed by Alsanat et al. [17] and validated herein against the ultimate web crippling capacities acquired from the experimental tests and parametric analyses. This equation has the ability to predict the web crippling strengths of both roll-formed aluminium and cold-formed steel lipped channel sections [17].

$$P_{unified} = Ct^2\sqrt{Ef_y}\sin\theta\left(1 - C_R\sqrt{\frac{r_i}{t}}\right)\left(1 + C_N\sqrt{\frac{N}{t}}\right)\left(1 - C_h\sqrt{\frac{h}{t}}\right) \quad (10)$$

The mean and the corresponding COV values of the ultimate-to-unified web strengths are 1.04 and 0.10, respectively, for the ETF loading condition, whereas these values are 1.08 and 0.07 for the ITF loading condition as shown in Table 6. Therefore, Equation (10) is further proven to have the ability to estimate the web crippling strengths of wide-ranged ALC sections with satisfactory COV values. Figures 16 (a) and (b) show the comparison between the crippling

capacities values ($P_{predicted}$) yielded by the aforementioned modified design rules and the ultimate capacities ($P_{Exp.-FEA}$) acquired from the experiments and numerical analysis under the ETF and ITF loading conditions, respectively.

6 The proposed Direct Strength Method (DSM)-based capacity prediction approach

The Direct Strength Method (DSM) is a useful and reliable design approach developed by Schafer [25] to predict the ultimate strengths based on the elastic and plastic capacities of thin-walled sections. Recently, the DSM has been accepted by the AS/NZS 4600 Standards [19] for cold-formed steel structures under compression, bending and shear actions. However, no DSM-based approach is available for the design of thin-walled sections subject to web crippling failure. Several attempts have been made to extend this method for cold-formed steel sections subjected to the web crippling action [26-32]. In this section, relevant equations reported in the literature to estimate the key parameters (elastic buckling and plastic loads) for thin-walled members were assessed. Subsequently, suitable improvements were made to develop a DSM design approach for ALC sections.

6.1 Critical buckling load

Generally, the elastic buckling load (P_{cr}) can be determined by a popularly used theoretical elastic buckling approach (Equation (11)) for conventional plates. However, due to the complex interface between the web, corner and the flange elements of the thin-walled members, such a simplified approach is rather inaccurate, therefore finite element or finite strip analyses are usually performed instead. For simplification, Sundararajah et al. [32] proposed an approach (Equation (12)) to determine the buckling coefficient (k_{cr}) for cold-formed steel lipped channel sections under the two flange loading conditions. Note that the coefficient (k_{cr}) has an empirical nature as it is related to geometrical dimensions of the section and the bearing length.

$$P_{cr} = \frac{\pi^2 E k_{cr} t^3}{12(1-\upsilon^2)d} \tag{11}$$

$$k_{cr} = C_b \left(1 - C_{b,r}\sqrt{\frac{r_i}{t}}\right)\left(1 - C_{b,w}\sqrt{\frac{h}{t}}\right)\left(1 + C_{b,N}\sqrt{\frac{N}{t}}\right)\left(1 + C_{b,b}\sqrt{\frac{b_f}{t}}\right) \tag{12}$$

where, C_b, $C_{b,r}$, $C_{b,w}$, $C_{b,\ell}$ and $C_{b,b}$ are the geometrical buckling coefficients for lipped channel sections (Table 7), and υ is the Poisson ratio (0.33 for aluminium).

To verify the suitability of Equation (12) for ALC sections under the ETF and ITF loading conditions, idealised numerical models were analysed using elastic buckling analyses for the 38 ALC test specimens. The elastic buckling coefficient ($k_{cr(FEA)}$) obtained by Equation (11) using the elastic buckling loads ($P_{cr(FEA)}$) acquired from the FE analyses were then compared with the estimation of Equation (12). A good agreement between the FE analyses results and the predictions using Sundararajah et al.'s [32] bucking coefficient k_{cr} were found. The mean and COV values of $k_{cr(FEA)}$ to k_{cr} are 1.00 and 0.09 for the ETF loading condition, respectively, while these values are 0.95 and 0.07 for the ITF load case, as shown in Table 8. Hence the critical elastic buckling coefficient (k_{cr}) calculated using Equation (12) was considered suitable to predict the elastic buckling load of the ALC sections.

6.2 Plastic load

Determining the plastic/yield load (P_y) is rather complex since the web crippling mechanism is associated with localised deformations and non-uniform distribution of the stresses. Yield-line Theory (YLT) was employed by Zhou and Young [33] and Natário et al. [28, 29] to estimate the plastic load of thin-walled members (Equation (13)). Zhou and Young [33] developed analytical models to predict the yield load of hollow members subject web crippling. In this model, the plastic mechanism length (N_m) is determined according to the assumption of the load dispersion rate of 1:2.5 through the section corner, and 1:1 through the web for both the ETF and ITF loading conditions. Natário et al. [28, 29] further amended this assumption by increasing the load dispersion rate through the web from 1:1 to 1:1.5 for the ITF loading condition and maintained the same assumption for the ETF loading condition (Equations (14) and (15)). However, this assumption was deemed by Natário et al. [29] to be limited, as the plastic load in certain cases may not fit well with the actual failure mechanism. This was observed by Sundararajah et al. [10] as the ultimate loads obtained from the FE analyses for cold-formed lipped channel sections with high bent radius (r_i = 7 mm) exceeded the plastic load. Figures 17 (a) and (b) show the ultimate-to-plastic load ratio (P_n/P_y) data distributions of cold-formed steel (reported by Sundararajah et al. [10]) and ALC sections under the DSM-format. The plastic load was calculated according to the assumptions made by Natário et al. [28,29] (Equations (14) and (15)). A large number of data points (models with r_i = 7 and 8 mm) are found above the plastic plateau (P_n/P_y=1) for the ITF loading condition which is theoretically not acceptable regardless of the potential strain hardening effects [29]. Even for the ETF loading condition, the data points in the vicinity of the plastic plateau indicate that the

governing failure was mainly plastic (yielding) failure; however, it was observed from the FE analysis that the prominent failure was buckling for these points.

$$P_y = f_y N_m(\sqrt{4r_m^2 + t^2} - 2r_m) \quad (13)$$

$$N_m = N + 2.5r_{ext} + h/2 \quad \text{(ETF)} \quad (14)$$

$$N_m = N + 2(2.5r_{ext} + 3h/4) \quad \text{(ITF)} \quad (15)$$

where r_{ext} is the external bent radius (r_i+t), N_m is the yield mechanism length and r_m is the bent radius measured along the middle of the section (r_i+$t/2$).

To further comprehend the plastic mechanism for lipped channel sections with different corner radii, a rigid plastic numerical analysis was undertaken to estimate the plastic mechanism length. To observe a pure (rigid) plastic mechanism in the numerical analysis, the elastic buckling capacity of the sections was strengthened by assuming a large value for the elastic modulus ($E \to \infty$) and therefore the FE models were governed by plastic (yielding) failure. Figures 18 (a) and (b) show the von Mises stress distributions of the rigid 15030-N100 specimen with three different external corner radii (r_{ext} =5, 8, and 11 mm) under both the ETF and ITF loading conditions, respectively, at the ultimate load. It is clear that the non-uniform stresses largely distribute through the section corners which implies that the section external bent radius has a considerable influence on the plastic mechanism length of the section. The increase of the plastic mechanism length was found to be around 11 times the increase in the external corner radius (Δr), as shown in Figures 18 (a) and (b). Based on this observation, Equations (16) and (17) were proposed in this study to estimate the plastic mechanism length for both the ETF and ITF loading conditions, respectively. Note that Equation (13) proposed by Natário et al. [29] was used in this study to calculate the plastic load of unfastened lipped channel sections under the ETF and ITF loading conditions.

$$N_m = N + 11r_x + h/2 \quad \text{(ETF)} \quad (16)$$

$$N_m = N + 2(11r_x + 3h/4) \quad \text{(ITF)} \quad (17)$$

6.3 The proposed DSM-based design rules

In this research, a DSM-based approach was developed based on (i) the experimental and FE parametric analysis data obtained herein for aluminium sections (Table 4), (ii) the experimental and FE parametric analysis data reported by Sundararajah et al. [10] for cold-formed steel

lipped channel sections (252 ETF and 252 ITF models), (iii) the critical buckling load calculated using Equations (11) and (12), and (iv) the yield load calculated using Equations (13), (16) and (17). Using a non-linear regression analysis, the DSM design formulae (Equations (18) and (19)) were calibrated based on (i) and (ii) data to estimate the ultimate web crippling strengths (P_n) of the lipped channel sections, and the coefficients of determination are R^2=0.94 and R^2=0.90 for the ETF and ITF loading conditions, respectively.

For the ETF loading condition:

$$P_n = \begin{cases} P_y & \text{for } \lambda \leq 0.43 \\ 0.57P_y\left[1 - 0.14\left(\frac{P_{cr}}{P_y}\right)^{0.67}\right]\left(\frac{P_{cr}}{P_y}\right)^{0.67} & \text{for } \lambda > 0.43 \end{cases} \quad (18)$$

For the ITF loading condition:

$$P_n = \begin{cases} P_y & \text{for } \lambda \leq 057 \\ 0.89P_y\left[1 - 0.222\left(\frac{P_{cr}}{P_y}\right)^{0.75}\right]\left(\frac{P_{cr}}{P_y}\right)^{0.75} & \text{for } \lambda > 0.57 \end{cases} \quad (19)$$

where λ is the web crippling slenderness ($\lambda = \sqrt{P_y/P_{cr}}$).

Figures 19 (a) and (b) present the ultimate-to-plastic load ratio P_n/P_y (representing the strength reduction factor) versus the web crippling slenderness (λ). According to these results, a well-defined trend signifying the relationship between the P_n/P_y and the web crippling slenderness (λ) is clearly visible for both the ETF and ITF loading conditions. It is also observed that the data points are situated under the plastic plateau (i.e., P_n/P_y=1) for both loading conditions. This generally indicates the adoption of reliable proposed Yield-line Theory (YLT) models, associated with the calculation of the plastic load (P_y) as discussed in Section 6.2. As expected, it was found that the stocky sections (i.e., low *h/t*) with large inside bent radii (r_i) are mostly governed by yielding (closer to the plastic plateau) owing to their high elastic buckling capacity, whereas slender sections (i.e., high *h/t*) with small r_i often fail in elastic buckling. Moreover, the high accuracy and reliability of the proposed DSM design equations for both the aluminium and steel lipped channel sections as evident in Figure 19, verifying the strong capability of the proposed DSM-based approach to be applied to different material types. The mean and COV values of $P_{Exp.\text{-}FEA}/P_{predicted}$ (predictions by the proposed DSM-based approach) capacity ratios are 1.04 and 0.14 for the ETF loading conditions, while these values are 1.03 and 0.16 for the ITF loading condition, as given in Table 6.

7 Reliability analysis

The resistance factor(ϕ_w) can be determined using a statistical model provided in the North American Specification [34]. This model considers the variation in loading, fabrication and material effects. The capacity resistance factor is given by Equation (20a).

$$\phi_w = 1.5 M_m F_m P_m e^{-\beta_0 \sqrt{V_M^2 + V_F^2 + C_n V_P^2 + V_Q^2}} \quad (20a)$$

where ϕ_w is the resistance factor; M_m, V_m = 1.1, 0.06 are, respectively, the mean value and coefficient of variation of the material factor; F_m and V_F = 1.0, 0.05 are, respectively, the mean value and COV of the fabrication factor; P_m and V_P are, respectively, the mean value and the coefficient of variation of the test-to-predicted load ratio; β_0 = 2.5 is the target reliability index for beams; $C_n = n^2 - 1/n^2 - 3n$ is the correction factor depending on the number of tests *n*; $V_Q =$ 0.21 is the coefficient of variation of the load effect.

All the above values can be substituted into Equation (20a) to yield the following equation.

$$\phi_w = 1.65 P_m e^{-2.5 \sqrt{0.0502 + C_n V_P^2}} \quad (20b)$$

Equation (20b) was used to calculate the resistance factors for the strength values predicted from the international design codes, the modified design rules [17] as well as the proposed DSM-based design approach. As shown in Table 6, the resistance factors (ϕ_w) obtained from the modified equations range between 0.90 and 0.97. Therefore, it is recommended to use a ϕ_w factor of 0.90 for all the modified equations. In addition, a ϕ_w factor of 0.85 is suggested when the proposed DSM-based approach is used to predict the web crippling strengths of cold-formed steel and ALC sections under the ETF and ITF loading conditions.

8 Conclusions

A numerical study conducted on roll-formed ALC sections subject to web crippling failure under the ETF and ITF loading conditions was presented in detail. Thirty-eight numerical models were developed and compared with the experimental results. A wide-ranging parametric study was then performed based on the validated numerical models to further investigate a wide range of geometrical parameters and different aluminium alloy grades. Firstly, it was found that the AISI standard test method limitations in terms of the specimen length $L \geq 5d$ for ITF loading condition may not be applicable for aluminium members, therefore the specimen length control $L \geq 6d$ is recommended. Subsequently, the acquired large database containing FE analysis and experiment results was used to evaluate the

consistency and reliability of the current design rules recommended by the international specifications, and the accuracy of the modified equations. It is shown that the design guidelines given in the international specifications highly overestimate the actual web crippling capacities with a large coefficient of variation (COV). On the other hand, the modified equations are capable to reasonably predict the web crippling strengths of the ALC sections under two-flange loading conditions. This study also presents a first attempt to apply a DSM-design approach to determine the web crippling capacities for roll-formed aluminium sections. Elastic buckling analysis was carried out to validate the approach proposed in the literature to predict the buckling load for the aluminium members. FE rigid plastic analysis was also performed to develop a reliable approach to estimate the plastic mechanism length associated with the determination of the plastic load. The proposed DSM-based approach was then validated against the FE and experimental data of both roll-formed aluminium and cold-formed steel lipped channel sections with good agreements.

Acknowledgement

The authors wish to thank Griffith University for providing the necessary technical support and test facilities, Mr Robert Price from BlueScope Building Components Pty Ltd for supplying the test specimens and Dr Lavan Sundararajah for providing his parametric data for use in this study.

References

[1] G. De Matteis, G. Brando, F.M. Mazzolani, Pure aluminium: An innovative material for structural applications in seismic engineering, Constr. Build. Mater. 26 (2012) 677-686. https://doi.org/10.1016/j.conbuildmat.2011.06.071.

[2] P. Zhu, H. Fan, Y. Zhou, Flexural behavior of aluminum I-beams strengthened by pre-stressed CFRP tendons, Constr. Build. Mater. 122 (2016) 607-618. https://doi.org/10.1016/j.conbuildmat.2016.06.115.

[3] F. M. Mazzolani, Structural applications of aluminium in civil engineering, Struct. Eng. Intern. 16 (2006) 280-285. https://doi.org/10.2749/101686606778995128.

[4] X. Guo, L. Wang, Z. Shen, J. Zou, L. Liu, Constitutive model of structural aluminum alloy under cyclic loading, Constr. Build. Mater. 180 (2018) 643-654. https://doi.org/10.1016/j.conbuildmat.2018.05.291.

[5] M. Macdonald, M.H. Don, M. KoteŁko, J. Rhodes, Web crippling behaviour of thin-walled lipped channel beams, Thin-Walled Struct. 49 (2011) 682-690. https://doi.org/10.1016/j.tws.2010.09.010.

[6] W.X. Ren, S.E. Fang, B. Young, Finite-element simulation and design of cold-formed steel channels subjected to web crippling, J Struct. Eng. 132 (2006) 1967-1975. https://doi.org/10.1061/(ASCE)0733-9445(2006)132:12(1967).

[7] A. M. Yousefi, J. B. Lim, G. C. Clifton, Cold-formed ferritic stainless steel unlipped channels with web perforations subject to web crippling under one-flange loadings, Constr. Build. Mater. 191 (2018) 713-725. https://doi.org/10.1016/j.conbuildmat.2018.09.152.

[8] P. Natario, N. Silvestre, D. Camotim, Web crippling failure using quasi-static FE models, Thin-Walled Struct. 84 (2014) 34-49. https://doi.org/10.1016/j.tws.2014.05.003.

[9] L. Sundararajah, M. Mahendran, P. Keerthan, Web crippling studies of SupaCee sections under two flange load cases, Eng. Struct. 153 (2017) 582-597. https://doi.org/10.1016/j.engstruct.2017.09.058.

[10] L. Sundararajah, M. Mahendran, P. Keerthan, New design rules for lipped channel beams subject to web crippling under two-flange load cases, Thin-Walled Struct. 119 (2017) 421-437. https://doi.org/10.1016/j.tws.2017.06.003.

[11] T. Dokšanović, I., Džeba, D. Markulak, Applications of aluminium alloys in civil engineering, Tehnički vjesnik: znanstveno-stručni časopis tehničkih fakulteta Sveučilišta u Osijeku, 24 (2017) 1609-1618. https://doi.org/10.17559/TV-20151213105944.

[12] F. Zhou, B. Young, Aluminum tubular sections subjected to web crippling—Part I, Thin-Walled Struct. 46 (2008) 339-351. https://doi.org/10.1016/j.tws.2007.10.003.

[13] F. Zhou, B. Young, Web crippling of aluminium tubes with perforated webs, Eng. Struct. 32 (2010) 1397-1410. https://doi.org/10.1016/j.engstruct.2010.01.018.

[14] Y. Chen, X. Chen, C. Wang, Aluminum tubular sections subjected to web crippling, Thin-Walled Struct. 90 (2015) 49-60. https://doi.org/10.1016/j.tws.2015.01.009.

[15] Y.Q. Wang, Z.X. Wang, F.X. Yin, L. Yang, Y.J. Shi, J. Yin, Experimental study and finite element analysis on the local buckling behavior of aluminium alloy beams under concentrated loads, Thin-Walled Struct. 105 (2016) 44-56. http://dx.doi.org/10.1016/j.tws.2016.04.003.

671 [16] M.N. Su, B. Young, Design of aluminium alloy stocky hollow sections subjected to
672 concentrated transverse loads, Thin-Walled Struct. 124 (2018) 546-557.
673 https://doi.org/10.1016/j.tws.2017.12.015.

674 [17] H. Alsanat, S. Gunalan, H. Guan, P. Keerthan, J. Bull, Experimental study of aluminium
675 lipped channel sections subjected to web crippling under two flange load cases, Thin-
676 Walled Struct. 141 (2019) 460-476. https://doi.org/10.1016/j.tws.2019.01.050.

677 [18] Standards Australia (SA), Aluminium structures - Part 1: Limit state design, AS/NZS
678 1664.1, Sydney, Australia, 1997.

679 [19] Standards Australia (SA), Cold-formed steel structures, AS/NZS 4600, Sydney,
680 Australia, 2005.

681 [20] European Committee for Standardization (CEN), Design of steel structures - Part 1.3:
682 Cold-formed members and sheeting, EN 1993-1-3, Brussels, Belgium, 1997.

683 [21] American Iron and Steel Institute (AISI), Standard test method for determining the web
684 crippling strength of cold-formed steel beams, TS-9-05, DC, USA, 2008.

685 [22] Simulia. ABAQUS Standard User's Manual, Version 6.14, Rhode Island, USA; 2013.

686 [23] M.N. Su, B. Young, L. Gardner, The continuous strength method for the design of
687 aluminium alloy structural elements, Eng. Struct. 122 (2016) 338-348.
688 https://doi.org/10.1016/j.engstruct.2016.04.040.

689 [24] European Committee for Standardization (CEN), Design of aluminium structures - Part
690 1.4: Cold-formed structural sheeting, Eurocode 9, Brussels, Belgium, 2007.

691 [25] B. W. Schafer, The direct strength method of cold-formed steel member design, J.
692 Constr. Steel Res. 64 (2008) 766-778. https://doi.org/10.1016/j.jcsr.2008.01.022.

693 [26] P. Keerthan, M. Mahendran, E. Steau, Experimental study of web crippling behaviour
694 of hollow flange channel beams under two flange load cases, Thin-Walled Struct. 85
695 (2014) 207-219. https://doi.org/10.1016/j.tws.2014.08.011.

696 [27] P. Keerthan, M. Mahendran, Experimental study on web crippling strength of hollow
697 flange channels under end-one-flange and interior-one-flange load cases, Adv. Struct.
698 Eng. 19 (2016) 966-981. https://doi.org/10.1177/1369433216630462.

699 [28] P. Natário, N. Silvestre, D. Camotim, Direct strength prediction of web crippling failure
700 of beams under ETF loading, Thin-Walled Struct. 98 (2016) 360-374.
701 https://doi.org/10.1016/j.tws.2015.09.012.

[29] P. Natário, N. Silvestre, D. Camotim, Web crippling of beams under ITF loading: A novel DSM-based design approach. J. Constr. Steel Res. 128 (2017) 812-824. https://doi.org/10.1016/j.jcsr.2016.10.011.

[30] Li HT, Young B. Cold-formed ferritic stainless steel tubular structural members subjected to concentrated bearing loads, Eng. Struct. 145 (2017) 392-405. https://doi.org/10.1016/j.engstruct.2017.05.022

[31] S. Gunalan, M. Mahendran, Web crippling tests of cold-formed steel channels under two flange load cases, J. Constr. Steel Res. 110 (2015) 1-15. https://doi.org/10.1016/j.jcsr.2015.01.018

[32] L. Sundararajah, M. Mahendran, P. Keerthan, Experimental studies of lipped channel beams subject to web crippling under two-flange load cases, J. Struct. Eng. 142 (2016). https://doi.org/10.1061/(ASCE)ST.1943-541X.0001523

[33] F. Zhou, B. Young, Yield line mechanism analysis on web crippling of cold-formed stainless steel tubular sections under two-flange loading, Eng. Struct. 28 (2006) 880-892. https://doi.org/10.1016/j.engstruct.2005.10.021.

[34] American Iron and Steel Institute (AISI), Specifications for the cold-formed steel structural members, Cold-formed Steel Design Manual, AISI S100, Washington, USA, 2012.

(a) ETF test (b) ITF test (c) cross section

Figure 1: Web crippling test setup and ALC section profile [17]

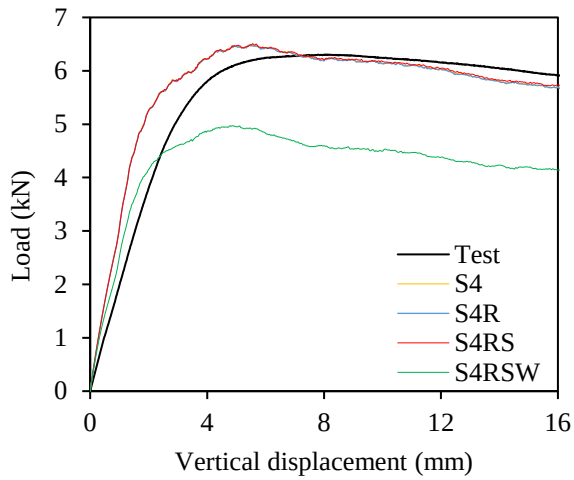

Figure 2: Load versus vertical displacement curves for different types of shell elements (ETF-10030-N50)

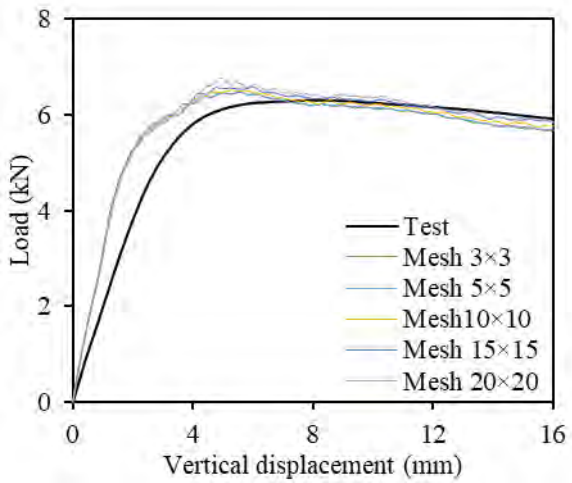

Figure 3: Load versus vertical displacement curves for different mesh sizes (ETF-10030-N50)

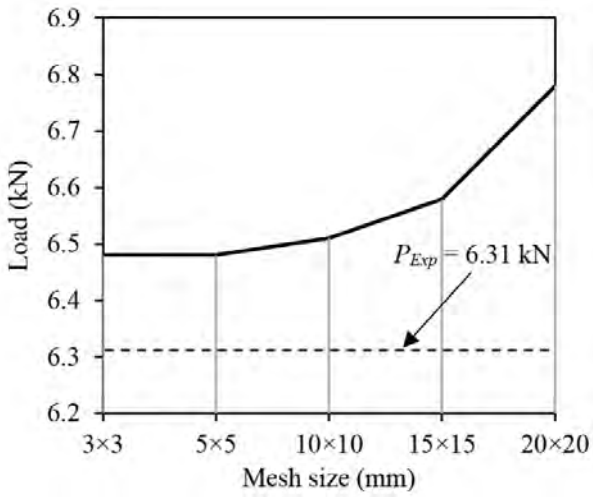

Figure 4: Ultimate load versus mesh size for ETF-10030-N50 specimen

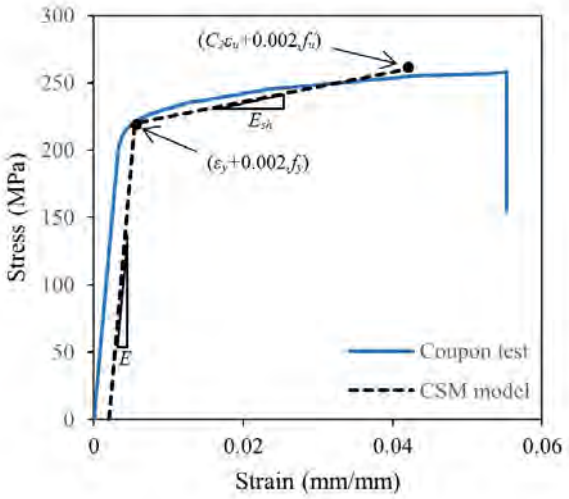

Figure 5: Typically measured stress-strain curve and the bi-linear CSM model for 5052-H36 aluminium alloy

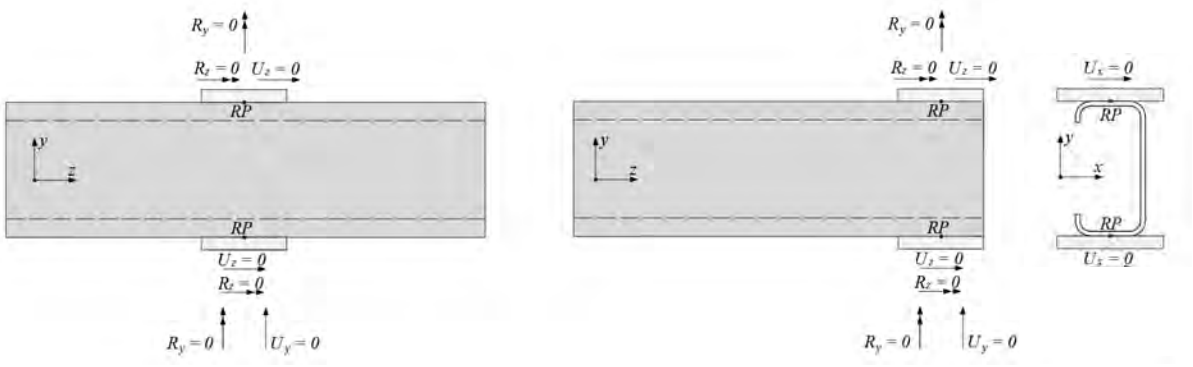

(a) Front view of ITF (b) Front view of ETF (c) Side view

Figure 6: Overview of the assigned boundary conditions in the web crippling models

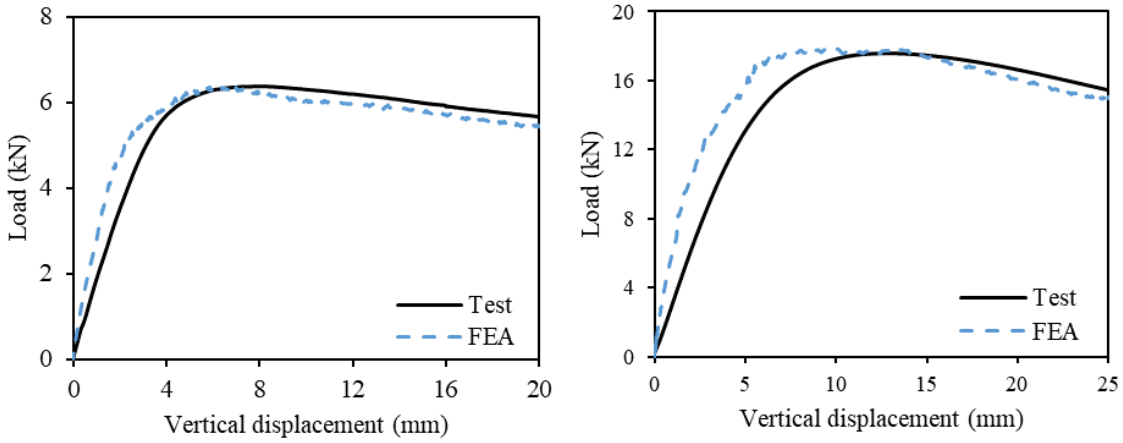

(a) ETF-15030-N100 (b) ITF-20030-N150

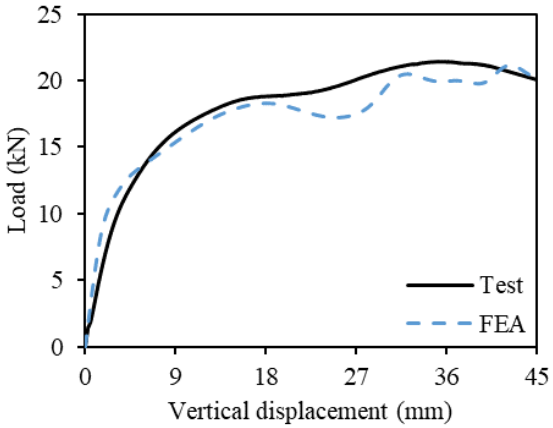

(c) ITF-15030-N25

Figure 7: Comparison of experimental and numerical load versus vertical displacement curves

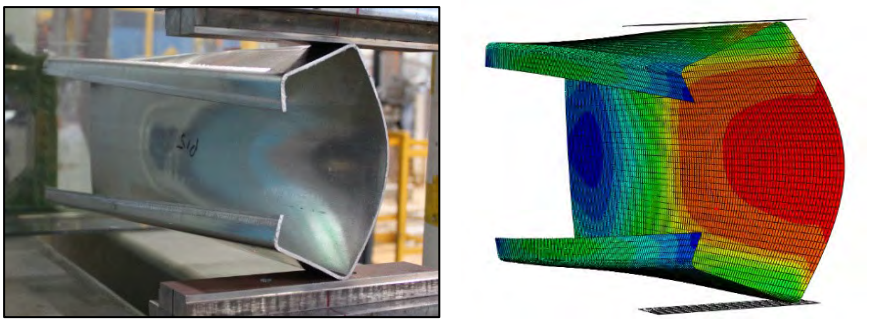

(a) Test specimen and FE model – ETF load case (ETF20025-N50)

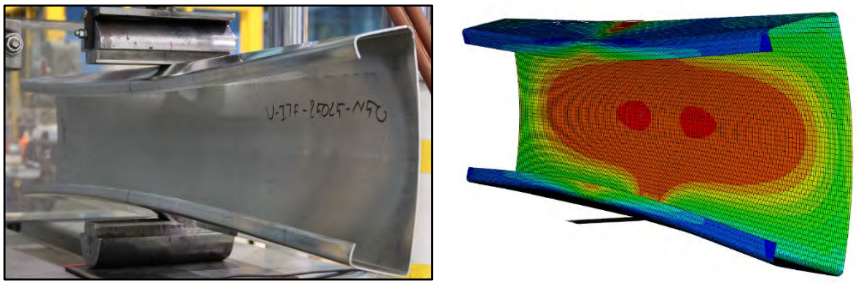

(b) Test specimen and FE model – ITF load case (ITF25025-N50)

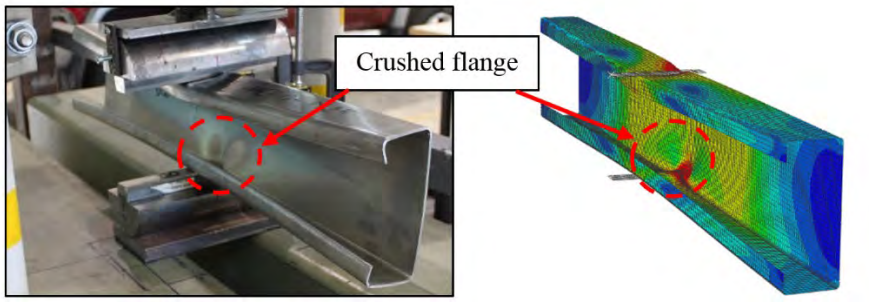

(c) Test specimen and FE model – ITF load case with flange crushing (ITF15030-N25)

Figure 8: Comparison of experimental and numerical failure modes

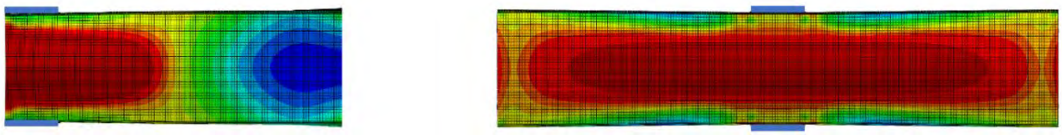

(a) ETF (L=3d) (b) ITF (L=5d)

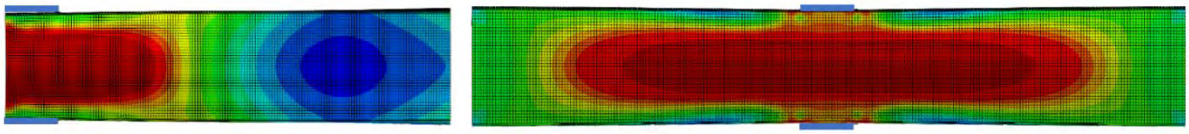

(c) ETF (L=4d) (d) ITF (L=6d)

Figure 9: von Mises stress distributions for 25025-N100 at the ultimate load

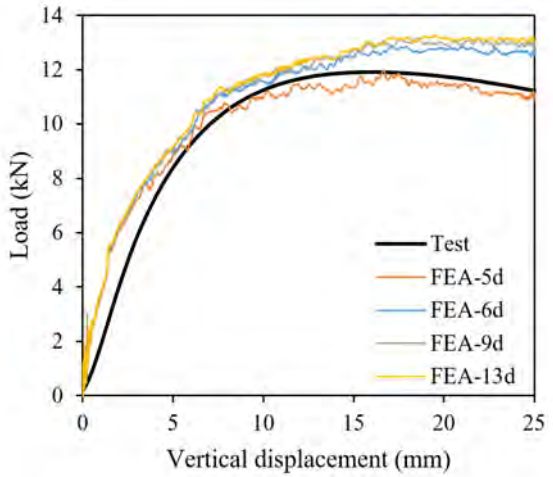

Figure 10: Load versus vertical displacement curves for specimen ITF-25025-N150 with different lengths

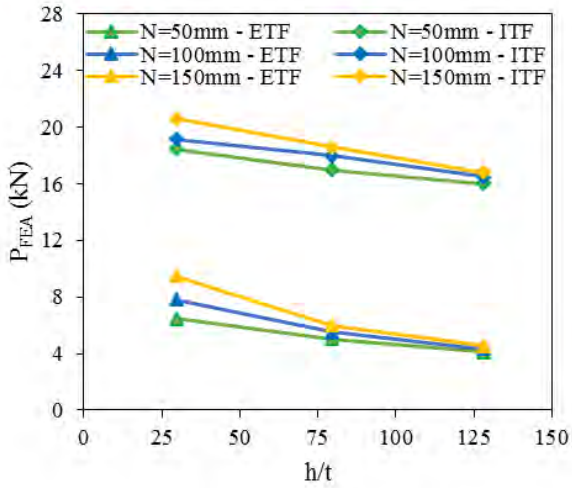

Figure 11: Web crippling capacity (P_{FEA}) versus web stiffness ratio (h/t) with different bearing lengths (models with r_i= 5 mm and f_y = 179 MPa)

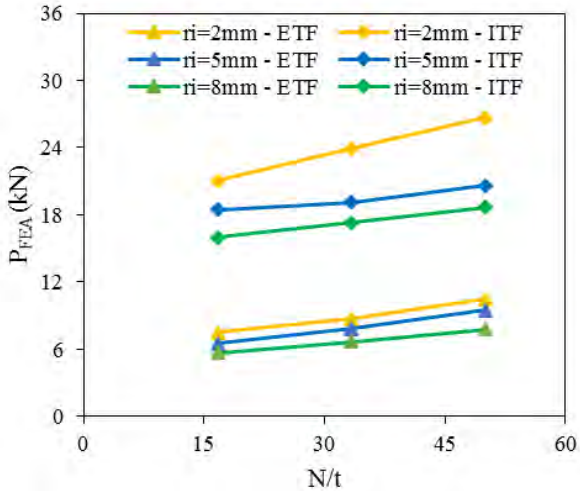

Figure 12: Web crippling capacity (P_{FEA}) versus bearing length ratio (N/t) with different inside bent radii (models with h/t = 32 and f_y =179 MPa)

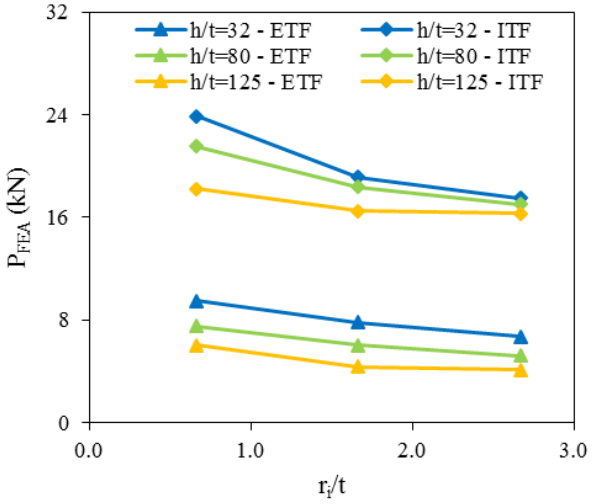

Figure 13: Web crippling capacity (P_{FEA}) versus inside bent radius ratio (r_i /t) with different web stiffness ratios (models with N = 100 mm and f_y =179 MPa)

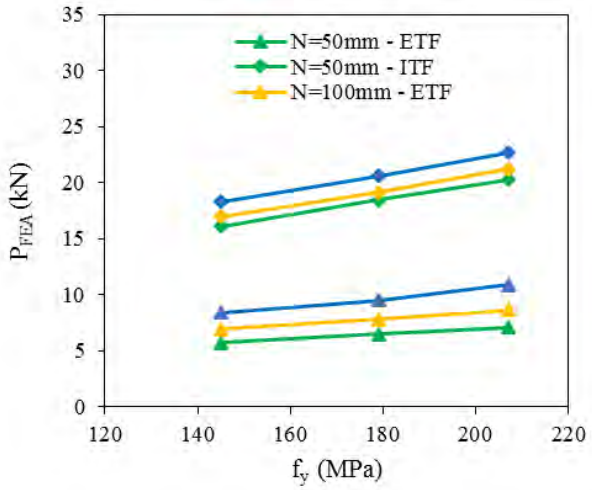

Figure 14: Web crippling capacity (P_{FEA}) versus yield stress (f_y) with different bearing lengths (models with h/t = 32 mm and r_i =5 mm)

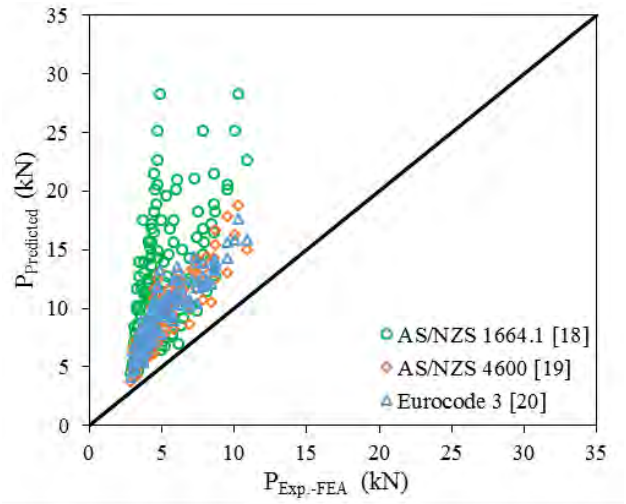

(a) ETF

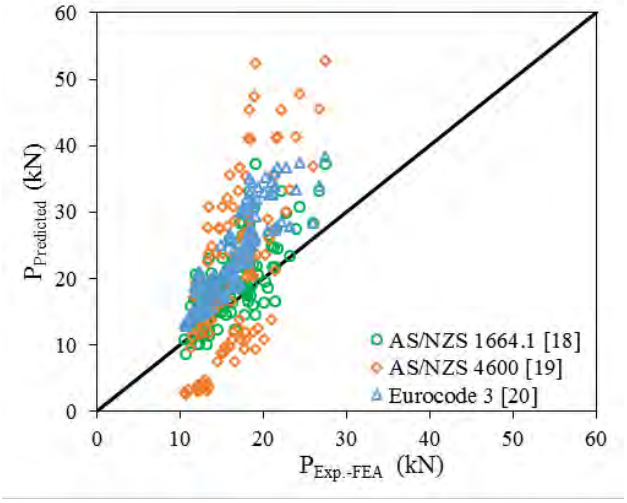

(b) ITF

Figure 15. Comparison between experimental and numerical capacities and predictions of international specifications

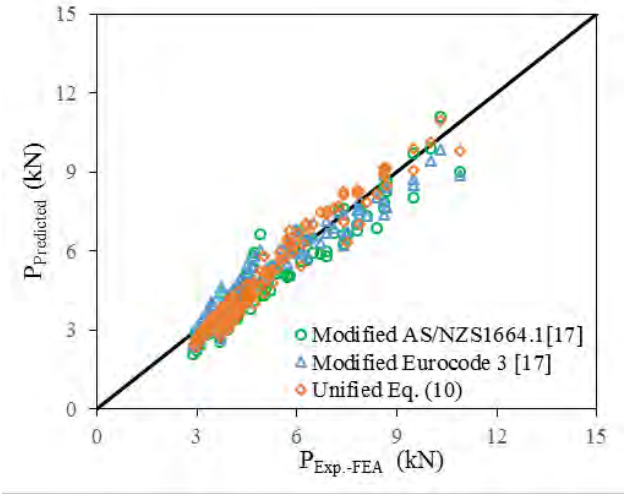

(a) ETF

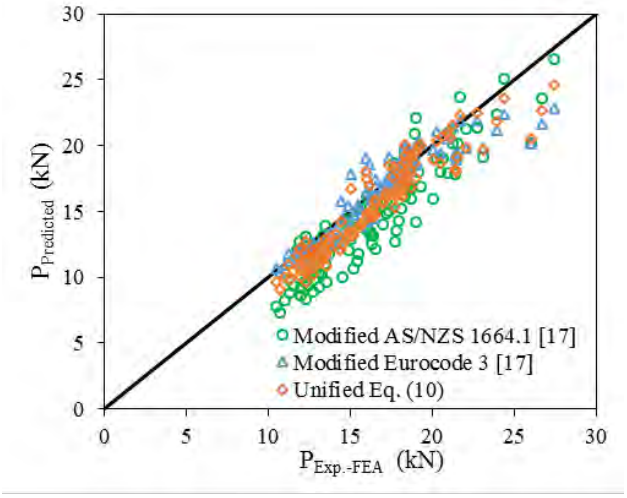

(b) ITF

Figure 16. Comparison between experimental and numerical capacities and predictions of recently modified equations [17].

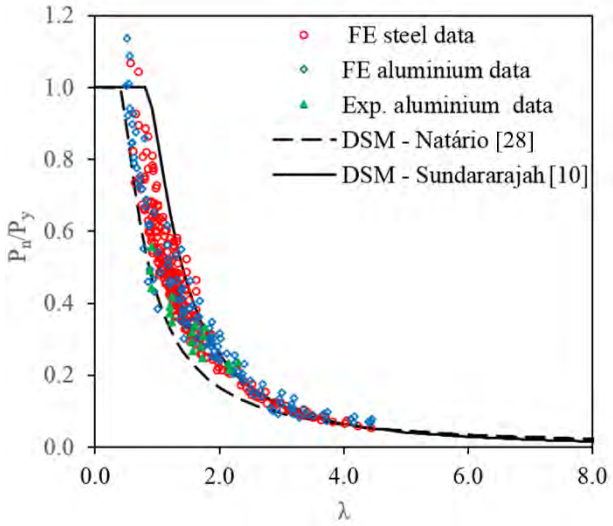

(a) ETF

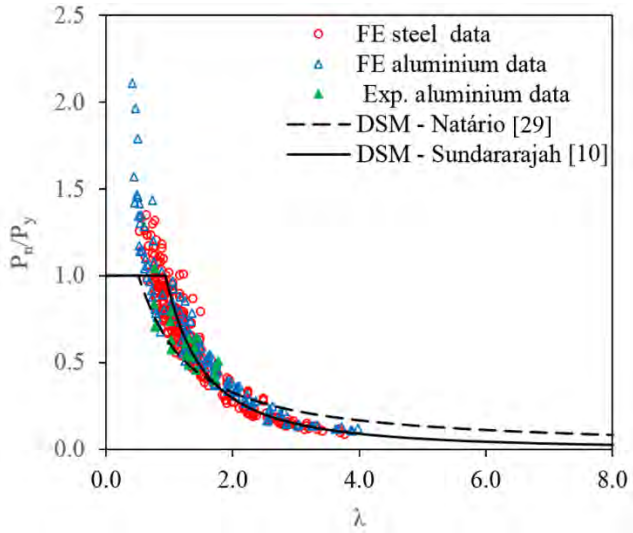

(b) ITF

Figure 17: P_n/P_y data distributions of cold-formed steel and ALC sections with DSM-based formulas under ETF and ITF load cases using the assumptions made by Natario et al. [28,29]

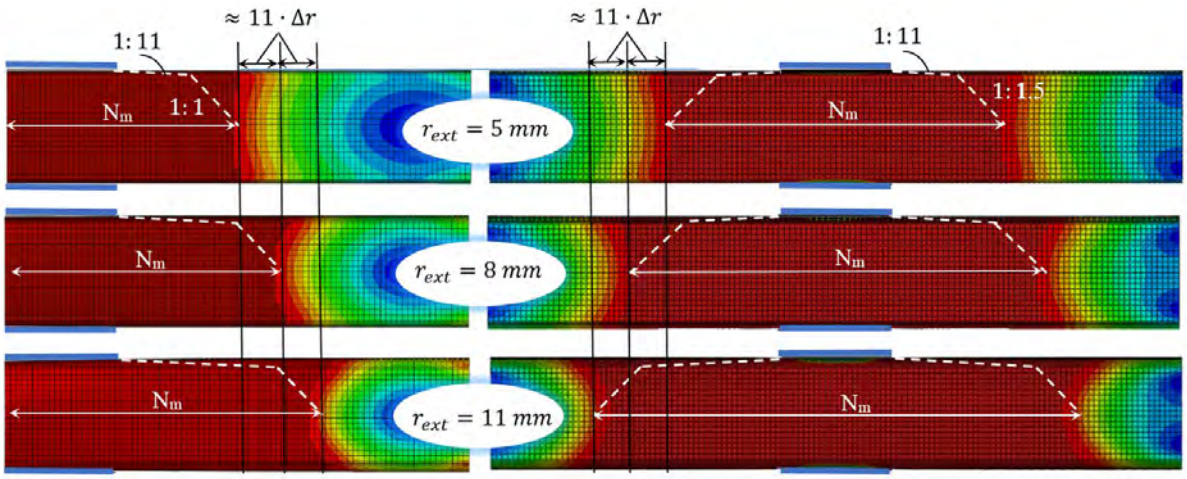

(a) ETF (b) ITF

Figures 18: von Mises stress distributions of 15030-N100 specimen with different external corner radii

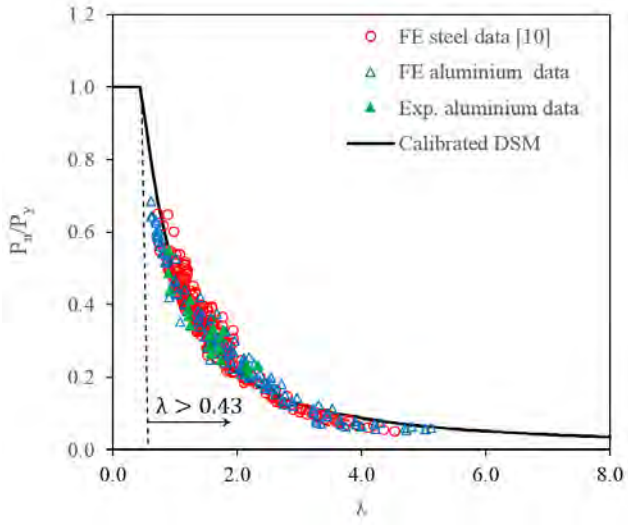

(a) ETF

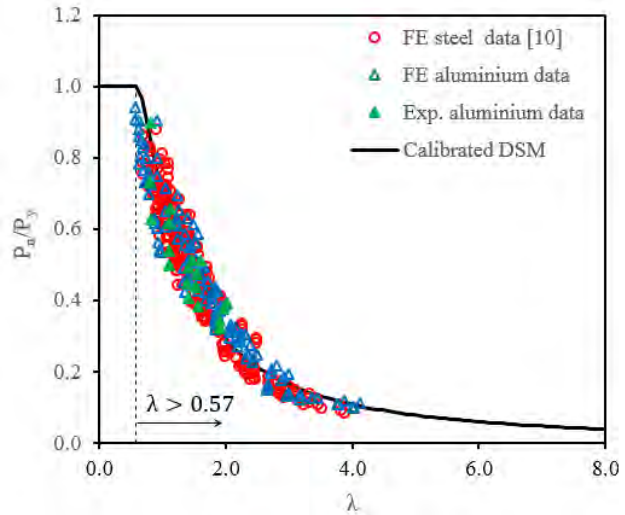

(b) ITF

Figure 19: Comparison between the proposed DSM curve and FE/experimental data from aluminium and steel section database

881 Table 1: Comparison of experimental and numerical web crippling capacities for ETF load case

Specimen	d (mm)	b_f (mm)	l_b (mm)	t (mm)	r_i (mm)	L (mm)	$P_{Exp.}$ (kN)	P_{FEA} (kN)	$P_{Exp.}/P_{FEA}$
ETF-10030-N25	107.3	60.4	14.9	2.95	4.9	316	6.19	5.85	1.06
ETF-10030-N50	106.5	58.4	16.1	2.95	5.0	317	6.23	6.46	0.97
ETF-10030-N100	107.3	59.4	15.0	2.95	4.8	316	7.41	7.83	0.95
ETF-15030-N25	156.7	62.8	22.9	2.93	4.9	466	5.23	5.41	0.97
ETF-15030-N50	157.5	63.3	22.4	2.93	5.0	465	5.50	5.74	0.96
ETF-15030-N100	158.3	63.5	21.7	2.92	5.1	465	6.37	6.48	0.98
ETF-15030-N150	155.5	63.5	22.9	2.92	4.9	467	7.25	7.62	0.95
ETF-20025-N25	208.1	74.6	25.5	2.42	5.1	617	3.33	3.34	1.00
ETF-20025-N50	208.1	74.2	25.4	2.43	4.9	615	3.61	3.48	1.04
ETF-20025-N100	207.3	74.3	25.7	2.43	5.0	615	3.92	3.78	1.04
ETF-20025-N150	204.0	75.8	26.5	2.43	4.8	615	4.23	4.30	0.98
ETF-20030-N25	204.6	74.9	27.4	2.9	4.6	611	4.95	5.11	0.97
ETF-20030-N50	208.4	73.0	27.5	2.9	5.0	615	5.07	5.22	0.97
ETF-20030-N100	204.5	75.4	27.7	2.89	4.6	613	5.82	5.91	0.98
ETF-20030-N150	208.3	73.5	27.1	2.89	5.0	615	6.06	6.40	0.95
ETF-25025-N25	259.8	80.8	23.4	2.43	4.4	765	2.95	3.01	0.98
ETF-25025-N50	259.9	76.1	23.7	2.44	4.9	765	3.09	3.11	0.99
ETF-25025-N100	262.1	76.2	22.7	2.44	4.8	765	3.76	3.36	1.12
ETF-25025-N150	260.3	76.3	23.4	2.45	4.6	765	4.15	3.69	1.12
Mean									1.00
COV									0.05

882

883 Table 2: Comparison of experimental and numerical web crippling capacities for ITF load case

Specimen	d (mm)	b_f (mm)	l_b (mm)	t (mm)	r_i (mm)	L (mm)	$P_{Exp.}$ (kN)	P_{FEA} (kN)	$P_{Exp.}/P_{FEA}$
ITF-10030-N25	106.9	59.3	14.3	2.94	4.8	527	21.40	22.05	0.97
ITF-10030-N50	106.4	59.4	14.8	2.95	4.9	525	18.57	18.00	1.03
ITF-10030-N100	106.1	59.6	14.4	2.94	4.8	523.5	18.29	18.57	0.98
ITF-15030-N25	156.5	62.6	22.6	2.93	4.8	774	18.71	18.49	1.01
ITF-15030-N50	156.7	62.4	22.7	2.92	4.9	775	18.29	18.00	1.02
ITF-15030-N100	156.2	62.1	22.7	2.92	4.8	776	18.00	18.45	0.98
ITF-15030-N150	156.6	62.5	22.8	2.93	4.9	774	18.30	19.35	0.95
ITF-20025-N25	206.2	74.0	26.3	2.43	4.6	1028	12.82	12.39	1.03
ITF-20025-N50	207.2	73.3	26.0	2.44	4.9	1022	12.23	12.55	0.97
ITF-20025-N100	207.3	73.9	26.3	2.43	5.0	1019	12.19	12.32	0.99
ITF-20025-N150	207.4	73.4	26.9	2.44	4.6	1021	12.27	12.53	0.98
ITF-20030-N25	205.6	74.5	31.6	2.9	4.4	1022	18.12	18.43	0.98
ITF-20030-N50	206.6	75.3	27.4	2.93	4.8	102	18.00	18.50	0.97
ITF-20030-N100	206.5	74.4	26.7	2.9	4.8	1021	17.59	17.74	0.99
ITF-20030-N150	206.5	74.5	26.7	2.89	4.6	1022	17.62	19.35	0.91
ITF-25025-N25	259.9	76.1	22.1	2.43	4.4	1273	12.08	11.81	1.02
ITF-25025-N50	260.0	76.0	22.4	2.42	4.5	1274	11.79	11.58	1.02
ITF-25025-N100	259.8	76.3	22.5	2.43	4.5	1269	11.77	11.73	1.00
ITF-25025-N150	259.9	76.2	22.2	2.43	4.5	1275	11.91	11.97	0.99
Mean									1.00
COV									0.03

884

885

886 Table 3: Predicted ultimate web crippling capacities of specimens with different lengths for ITF load case

Specimen	Ultimate web crippling capacity (P_{FEA})						
	L=5d (kN)	*5d/13d* (%)	*L=6d* (kN)	*6d/13d* (%)	*L=9d* (kN)	*9d/13d* (%)	*L=13d* (kN)
ITF10030N100	18.63	0.94	19.76	0.99	19.91	1.00	19.90
ITF15030N100	18.45	0.94	19.22	0.98	19.54	0.99	19.70
ITF15030N150	19.35	0.94	20.09	0.97	20.42	0.99	20.66
ITF20025N100	13.01	0.88	14.38	0.97	14.65	0.99	14.85
ITF20025N150	13.41	0.88	14.74	0.97	15.00	0.98	15.28
ITF20030N100	17.79	0.90	19.29	0.98	19.49	0.99	19.67
ITF20030N150	17.89	0.90	19.49	0.98	19.74	0.99	19.93
ITF25025N100	11.77	0.90	12.84	0.98	13.11	1.00	13.12
ITF25025N150	11.97	0.90	12.89	0.97	13.18	0.99	13.27

887

888

889 Table 4: Parametric study model details of ALC sections under ETF and ITF load cases

Load case	Section	*h/t*	*N* (mm)	r_i (mm)	f_y (MPa)	Number of models
ETF	10030	31.7 - 27.7	50,100,150	2, 5, 8	145,179,207	27
	15025	53.6 - 58.4	50,100,150	2, 5, 8	179	9
	25025	96 - 98.4	50,100,150	2, 5, 8	145,179,207	27
	25030	77.7 - 81.7	50,100,150	2, 5, 8	179	9
	30025	110.6 - 116.4	50,100,150	2, 5, 8	179	9
	40030	126 -130	50,100,150	2, 5, 8	145,179,207	27
	Experiment					19
	FE-validation					19
	Sub-total					146
ITF	10030	31.7 - 27.7	50,100,150	2, 5, 8	145,179,207	27
	15025	53.6 - 58.4	50,100,150	2, 5, 8	179	9
	25025	96 -98.4	50,100,150	2, 5, 8	145,179,207	27
	25030	77.7 - 81.7	50,100,150	2, 5, 8	179	9
	30025	110.6 - 116.4	50,100,150	2, 5, 8	179	9
	40030	126 -130	50,100,150	2, 5, 8	145,179,207	27
	Experiment					19
	FE-validation					19
	Sub-total					146
Total						292

890

891

892

893

894

895

896

897 Table 5: Geometrical coefficients used in the AS/NZS 4600 [19] Standard and unified Equation (10)

Equation	Load case	C	C_R	C_N	C_h	ϕ_w
AS/NZS 4600 [19]	ETF	13	0.32	0.05	0.04	0.90
	ITF	24	0.52	0.15	0.001	0.80
Equation (10) [17]	ETF	0.273	0.21	0.16	0.06	0.90
	ITF	0.78	0.17	0.04	0.03	0.90

898

899 Table 6: Comparison of mean and COV values of web crippling capacity ratios $P_{Exp.\text{-}FEA}/P_{predicted}$

900

Design rules	Load case	Equations	Mean	COV	ϕ_w
Current [18-20]	ETF	AS/NZS 1664.1	0.44	0.35	0.25
		AS/NZS 4600	0.57	0.16	0.47
		Eurocode 3	0.54	0.14	0.46
	ITF	AS/NZS 1664.1	0.88	0.20	0.67
		AS/NZS 4600	0.89	0.47	0.40
		Eurocode 3	0.72	0.13	0.62
Modified [17]	ETF	AS/NZS 1664.1	1.07	0.11	0.94
		Eurocode 3	1.00	0.09	0.90
		Unified	1.04	0.10	0.92
	ITF	AS/NZS 1664.1	1.10	0.12	0.97
		Eurocode 3	1.03	0.07	0.94
		Unified	1.08	0.07	0.96
Proposed	ETF	DSM approach	1.04	0.14	0.89
	ITF	DSM approach	1.03	0.16	0.85

901
902

903 Table 7: Geometrical coefficients for the buckling coefficient (k_{cr}) [32]

Load case	C_b	$C_{b,r}$	$C_{b,w}$	$C_{b,l}$	$C_{b,b}$
ETF	0.58	0.01	0.05	0.30	0.05
ITF	1.84	0.01	0.03	0.10	0.05

904

905

906

907

908

909

910

911

912

913 Table 8: Critical buckling coefficient from FEA ($k_{cr(FEA)}$) and Equation (12) (k_{cr})

Section	ETF				ITF			
	$P_{cr(FEA)}$ (kN)	$k_{cr(FEA)}$	k_{cr}	$k_{cr(FEA)}/k_{cr}$	$P_{cr(FEA)}$ (kN)	$k_{cr(FEA)}$	k_{cr}	$k_{cr(FEA)}/k_{cr}$
10030-N25	13.05	0.91	0.95	0.96	33.98	2.38	2.39	0.99
10030-N50	17.30	1.19	1.13	1.06	36.03	2.49	2.62	0.95
10030-N100	24.15	1.68	1.39	1.21	40.19	2.79	2.94	0.95
15030-N25	7.60	0.81	0.86	0.93	22.31	2.36	2.29	1.03
15030-N50	9.16	0.98	1.03	0.95	23.45	2.51	2.50	1.01
15030-N100	12.18	1.32	1.27	1.04	25.01	2.67	2.81	0.95
15030-N150	15.88	1.69	1.45	1.16	26.88	2.85	3.04	0.94
20025-N25	3.06	0.76	0.79	0.96	9.71	2.36	2.24	1.05
20025-N50	3.57	0.88	0.95	0.92	10.09	2.44	2.46	0.99
20025-N100	4.64	1.13	1.18	0.96	10.44	2.55	2.78	0.92
20025-N150	5.92	1.42	1.37	1.04	10.97	2.65	3.02	0.88
20030-N25	5.31	0.75	0.80	0.93	16.53	2.35	2.23	1.05
20030-N50	6.05	0.87	0.95	0.92	17.12	2.37	2.44	0.97
20030-N100	7.93	1.13	1.18	0.96	17.14	2.45	2.73	0.90
20030-N150	9.63	1.40	1.34	1.05	17.96	2.59	2.96	0.88
25025-N25	2.31	0.70	0.72	0.98	7.17	2.19	2.14	1.02
25025-N50	2.65	0.80	0.86	0.93	7.23	2.23	2.36	0.95
25025-N100	3.25	0.99	1.06	0.93	7.59	2.31	2.66	0.87
25025-N150	4.48	1.33	1.22	1.09	7.78	2.37	2.90	0.82
Mean				1.00				0.95
COV				0.09				0.07

914

915